Fachtagung "Experimentelle Strömungsmechanik"
6.–8. September 2022, Ilmenau

Aerodynamic loads on and flow around velomobiles
Aerodynamische Kräfte an und Strömungen um Velomobile

Christof Gromke[1,*], Olivier Marzullo[1], Joachim Fuchs[2]

[1]Karlsruhe Institute of Technology KIT, Institute for Hydromechanics, Laboratory of Building and Environmental Aerodynamics, Karlsruhe, Germany

[2]Karlsruhe Institute of Technology KIT, Institute for Neutron Physics and Reactor Technology, Karlsruhe, Germany

[*]gromke@kit.edu

Key words: human powered vehicle, crosswind, Reynolds number sensitivity, sail effect
Schlagworte: Muskelkraftbetriebene Fahrzeuge, Seitenwind, Reynoldszahlempfindlichkeit, Segeleffekt

Abstract

Wind tunnel studies at two scaled models of velomobiles (fully-faired recumbent bikes) were performed. The models are replicas of an existing velomobile named 'Aeolos' and of one currently under design named 'Proton'. Force measurements were performed at the scaled models with a 3-axis force sensor for angles of wind attack ranging from 0° to 180° and for Reynolds numbers $0.2 \cdot 10^5 < Re < 1.7 \cdot 10^5$. For the velomobile 'Proton' additional flow field measurements at $Re = 0.94 \cdot 10^5$ at various angles of wind attack ranging from -30° to +30° were acquired with Particle Image Velocimetry (PIV).
A Reynolds number sensitivity study indicates largely independency of the drag coefficient for $Re > 0.9 \cdot 10^5$ for the model 'Aeolos' and for $Re > 1.2 \cdot 10^5$ for the model 'Proton' for most of the angles of wind attack. For both velomobiles, the drag coefficient C_d decreases with increasing apparent wind angle, becomes negative at around 30°, i.e. provides thrust due to a sail effect, and reaches a minimum at around 50° with $C_d = -0.51$ and $C_d = -0.63$ for 'Aeolos' and 'Proton', respectively, at $Re \approx 1.18 \cdot 10^5$ (the largest Re which could be realized at around 50° within this study). The PIV at the model 'Proton' indicates attached flow all along the top and side faces at zero angle of attack and a flow separation on the lateral face at two thirds of the length of the model, emerging at an angle of attack between 10° and 20°.

Introduction

Velomobiles are fully-faired recumbent or semi-recumbent bikes (Fig. 1) also referred to as human powered vehicles HPV (Rasmussen and Eick 2005). Due to their fairly streamlined shape, velomobiles experience considerably lower drag than other bicycle types. Drag coefficients of velomobiles are typically less than one fifth of those of cyclists riding in an upright sitting position. In addition, the frontal area of velomobiles can be 60% to 80% smaller than that of an upright sitting cyclist on a touring or city bike. Velomobile riders report that they can easily maintain riding velocities of around 50 km/h for one hour or more. However, riders also report a pronounced crosswind susceptibility of their velomobiles which is obviously attributable to their large lateral area of wind attack (Rasmussen, 2009; Weaver, 1994; Fuchs, 1998).
Nowadays, two basic categories of velomobiles can be distinguished; those which are intended for speed records and those which are intended for leisure time excursions or for everyday

GALA e.V., Karlsruhe, Germany, ISBN 978-3-9816764-8-8

use. The design of velomobiles of the first category is almost exclusively dominated by aerodynamic considerations with the aim of achieving an aerodynamic resistance as low as possible (Gross et al., 1983; Kyle and Weaver, 2004,). The velomobiles look similar to a torpedo with the rider being accommodated in a lying position and the cabin completely sealed. The current speed record with such a high-performance velomobile is 144.2 km/h and dates back to 2016 (IHPVA, 2019). Velomobiles of the second category may be realized as either recumbent or semi-recumbent versions, with the cabin accommodating the torso and the head of the rider being partly open or enclosed (Fig. 1). The design of velomobiles of this category includes next to aerodynamic considerations also aspects of safety, rideability, and occasionally also storage space for language. In any case, the aspect of aerodynamics plays a pivotal role in the design of velomobiles of either category. Tab. 1 provides an overview of aerodynamic characteristics and speed performance for selected bicycles types and HPVs.

Fig. 1: Different velomobile models for leisure time excursions or for everyday use; far right: 'Aeolos'.

Tab. 1: Aerodynamic characteristics and speed performance of different bicycle types and HPVs.

bicycle type or HPV name (category: r - racing, l - leisure)	year	drag coefficient C_d [-]	drag area $C_d \cdot A_{front}$ [m^2]	max. speed [km/h]
standard racing bicycle	-	0.9	0.32	-
touring bicycle	-	1.1	0.55	-
Vector Trike (r)	1980	0.11	0.046	94.8
Cutting Edge (r)	1989	0.11	0.029	120.2
Varna Diablo (r)	2001	-	0.020	129.6
Virtual Edge (r)	2002	0.045	0.014	125
Leitra (l)	1980	0.16	0.177	-
Aeolos (l)	1995	0.16	0.078	63
Quest (l)	2000	-	0.093	-
Mango (l)	2002	-	0.121	-

The present work addresses the aerodynamics of velomobiles intended for leisure time excursions or for everyday use. It examines two velomobile models, 'Aeolos' and 'Proton', which can be classified as fully-faired semi-recumbent single-track bikes with enclosed rider cabin.

Experiment Setup and Measurements

Wind Tunnel Facility and scaled Models of Velomobiles

The investigations were performed with geometrically scaled models (M = 1:10) of an existing single-track velomobile named 'Aeolos' - designed and built in the year 1995 - and of one currently under design named 'Proton', also single-track, placed on a splitter plate in the open measurement section of a Goettingen-type wind tunnel. The models were 3D-printed in polylactic acid (PLA), see Fig. 2. Their surfaces were sanded by successively applying finer sandpapers with a P1000 type in the final stage. Tab. 2 summarized geometric characteristics of the model velomobiles.

GALA e.V., Karlsruhe, Germany, ISBN 978-3-9816764-8-8

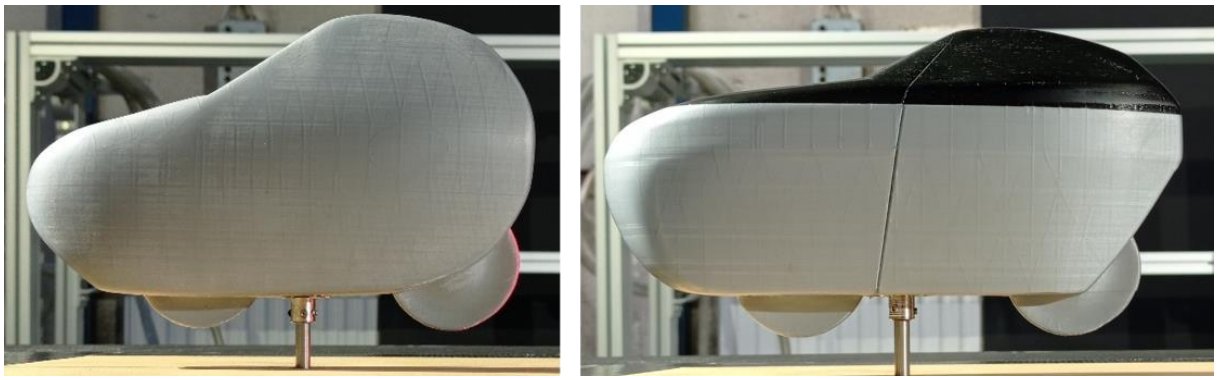

Fig. 2: Side view of model velomobile 'Aeolos' (left) and 'Proton' (right).

The wind tunnel studies were performed with free-stream velocities U_{fs} of the block-shape profile exiting the nozzle of the Goettingen-type wind tunnel in the range 5 m/s ≤ U_{fs} ≤ 35 m/s. The corresponding Reynolds numbers were in the range $0.2 \cdot 10^5 < Re < 1.7 \cdot 10^5$ for both models, with the Reynolds number based on the square root of the projected frontal area (A_{front}) of the model velomobiles at zero-incident angle as length scale. The turbulence intensity I_U of the approach flow was I_U ≤ 1%. More information on the experiment setup can be found in Marzullo (2022).

Tab. 2: Geometric characteristics of scaled model velomobiles.

velomobile model	scale	length [mm]	width (max) [mm]	height* [mm]	frontal area [mm²]	lateral area [mm²]
Aeolos	1:10	200	55	124	4,880	17,500
Proton	1:10	210	58	118	4,940	18,800

* including wheels

Force Measurements

A 3-axis force sensor (type K3D60a from ME-Meßsysteme GmbH) in combination with a tuned measurement amplifier (type GSV-4 from ME-Meßsysteme GmbH) including integrated temperature compensation was employed to measure the aerodynamic loads. The sensor has a measurement range of ±10 N and the accuracy is specified by the manufacturer to 0.5% (FS). Calibration and validation of the force measurement setup were performed several times throughout the entire experiment period. The signal acquisition was done with a sampling frequency of 125 Hz for a period of 30 s (Marzullo, 2022).

Velocity Measurements

Time-resolved Particle Image Velocimetry (2D2C PIV) was employed to acquire the flow field around the model velomobile 'Proton'. The PIV system encompasses a high-speed CMOS camera (Phantom v210), a 50 mm lens (Zeiss), and a pulsed dual-cavity Nd:YAG laser (Lee Laser) configured by Dantec Dynamics, see e.g. Gromke (2018) or Gromke and Ruck (2018) for more information on the PIV system and setup.
Velocity measurements were made at a free-stream velocity U_{fs} = 20 m/s ($Re = 0.94 \cdot 10^5$) in two acquisition planes, (i) in a vertical plane (x-z) aligned with the spanwise-central axis of the velomobile for approach flow under θ = 0° angle of attack, and (ii) in a horizontal plane (x-y) at the height of the maximum width of the velomobile for approach flows under angle of attack θ of 0°, ±10°, ±20°, and ±30° (Marzullo, 2022).
The PIV recordings were performed in the single-exposed double-frame mode with a sampling frequency of 1000 Hz (inter-frame time) over an acquisition time of 2.5 s. They were processed

GALA e.V., Karlsruhe, Germany, ISBN 978-3-9816764-8-8

and analysed with the software 'DynamicStudio' employing a two-step adaptive correlation method with final interrogation window size of 32 × 32 pixels by 50% overlap along both dimensions (Dantec Dynamics, 2013).

Results and Discussion

Force Coefficients

In Fig. 3 drag coefficients C_d for the velomobile 'Aeolos' obtained at the scaled model at approach flows with free-stream velocities 5 m/s ≤ U_{fs} ≤ 35 m/s ($0.2 \cdot 10^5$ < Re < $1.7 \cdot 10^5$) for various angles of attack θ are shown. The drag coefficient C_d was calculated according to

$$C_d = \frac{2\,F_d}{\rho\,V_a^2\,A_{fr,0}}$$

with F_d the measured time-mean force component in riding direction (drag force in body-axis system), ρ the density of air, V_a the apparent wind velocity, $V_a = U_{fs}$ in the wind tunnel experiments, and $A_{fr,0}$ the projected frontal area of the model velomobile at zero-incident angle.
A solid line to the left of the data points indicates drag coefficients which were determined based on measurements and a dashed line indicates coefficients obtained by extrapolation. The latter was done since the measurement range of the force sensor was exceeded at higher approach flow velocities for certain angles of attack. This implies that the drag coefficients with dashed lines to their left are estimations based on trend lines.

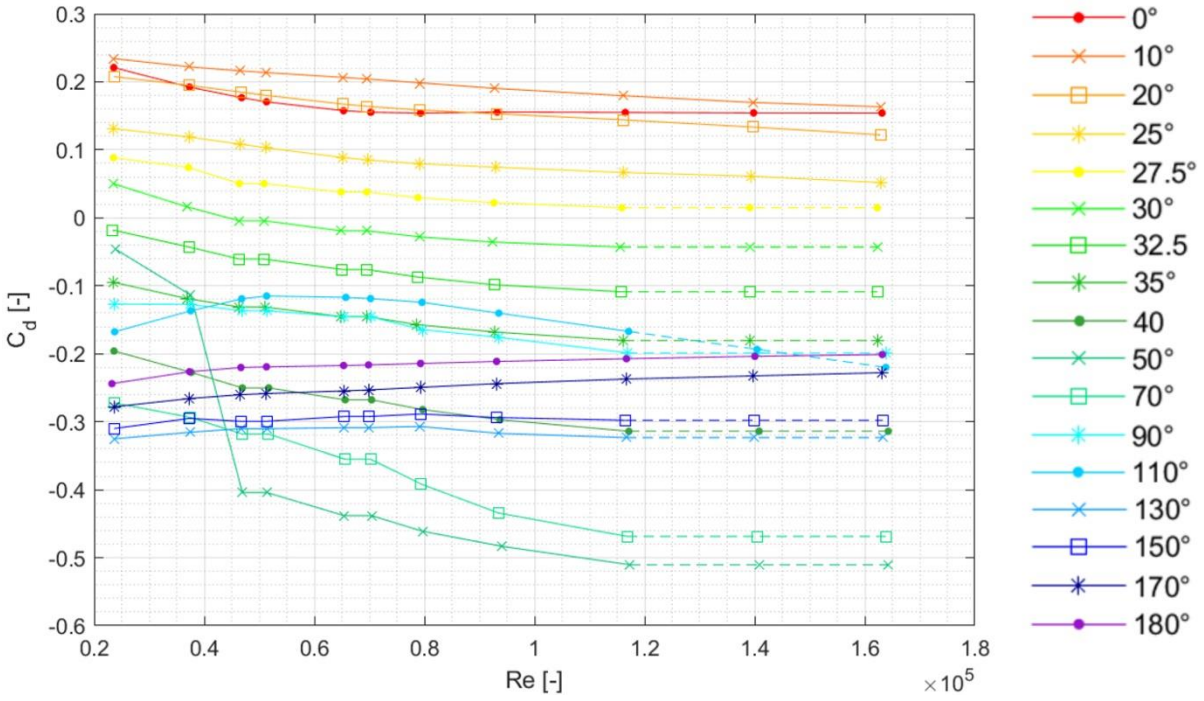

Fig. 3: Drag coefficients C_d of velomobile 'Aeolos' in dependency on Reynolds number Re for different angles of flow attack θ obtained at the scaled model.

Under head wind (θ = 0°), the drag coefficient of the velomobile 'Aeolos' is C_d = 0.16 at the largest Reynolds numbers investigated within this study. For comparison, the drag coefficient of a cyclist on a classical city bike in an upright sitting position is $C_d \approx 1.1$ and on a racing bike in a crouched position is $C_d \approx 0.9$, with frontal areas being approximately equal to and 70% of that of 'Aeolos', respectively. For most of the angles of wind attack θ, the drag coefficients appear to be fairly constant for Reynolds numbers Re > $0.9 \cdot 10^5$, i.e. at $U_{fs} \geq 20$ m/s. However,

GALA e.V., Karlsruhe, Germany, ISBN 978-3-9816764-8-8

the question whether or not a drag crisis, i.e. a relative abrupt decrease of the value of the drag coefficient analogue to that observed at e.g. a cylinder with a circular cross section or a sphere, occurs at higher Reynolds numbers cannot conclusively be answered based on the data provided in Fig. 3. Furthermore, the data in Fig. 3 exhibit an overall tendency of decreasing drag coefficient with increasing angle of wind attack for low to moderate angles ($\theta \leq 50°$). At $\theta = 32°$ the drag coefficient is always negative, independent of the Reynolds number, and at $\theta = 30°$ the drag coefficient is negative for $Re \geq 0.5 \cdot 10^5$, a Reynolds number which in full-scale is almost always exceeded during riding. Thus, a rider of the 'Aeolos' experiences thrust or a sail effect if the apparent wind comes from a direction of $\theta \geq 30°$. The change in sign of the drag coefficient for $\theta = 30°$ at $Re \approx 0.5 \cdot 10^5$ indicates a qualitative variation in the flow field around the velomobile. The maximum thrust for the angles of wind attack investigated herein was found at $\theta = 50°$. For $Re > 1.0 \cdot 10^5$ its absolute value is approximately 3 times that of the drag coefficient at head wind ($\theta = 0°$).
The drag coefficients C_d for the velomobile 'Proton' obtained at the scaled model at approach flows with free-stream velocities $5 \text{ m/s} \leq U_{fs} \leq 35 \text{ m/s}$ ($0.2 \cdot 10^5 < Re < 1.7 \cdot 10^5$) for various angles of attack are provided in Fig. 4.

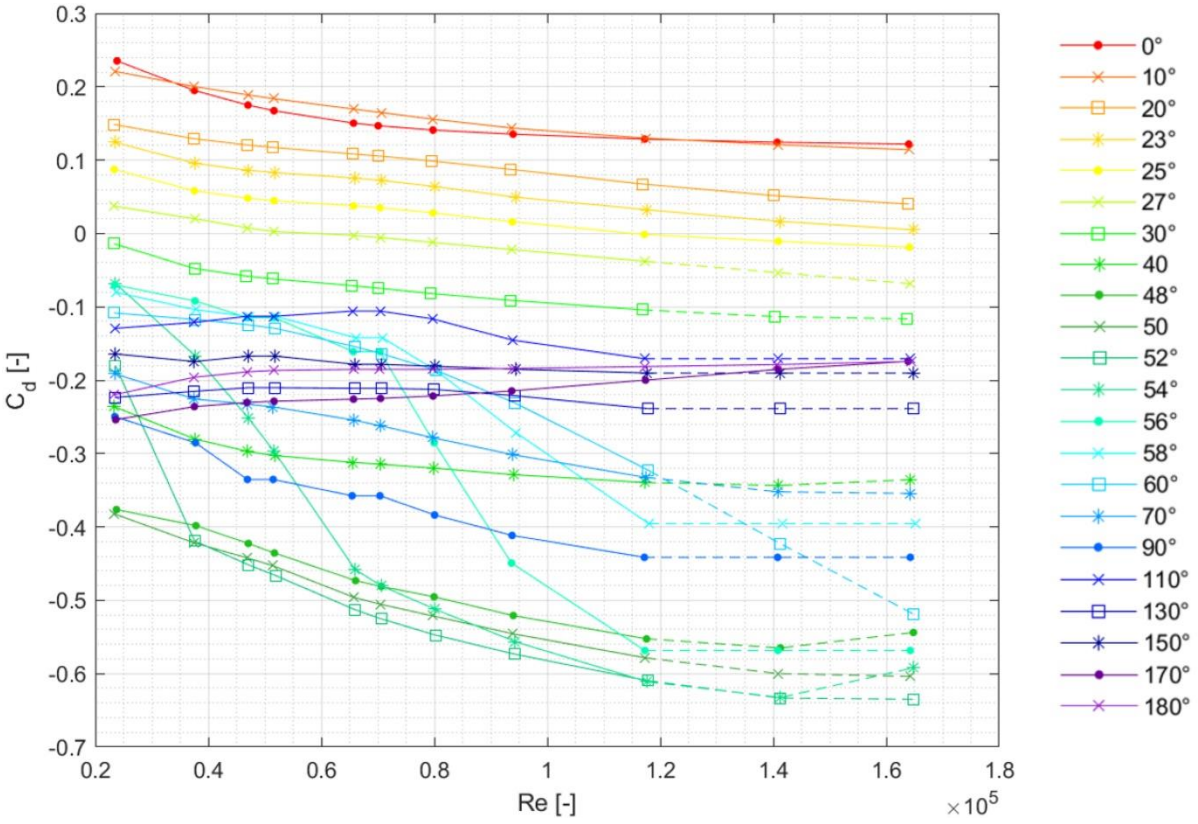

Fig. 4: Drag coefficients C_d of velomobile 'Proton' in dependency on Reynolds number Re for different angles of flow attack θ obtained at the scaled model.

Also in the case of the velomobile 'Proton', an independency of the drag coefficient at the largest Reynolds numbers tested within this study can be observed for most of the angles of wind attack θ. The threshold Reynolds number for a largely independency is estimated to $Re = 1.2 \cdot 10^5$, i.e. 20% to 30% larger than for the velomobile 'Aeolos'. The drag coefficient of the 'Proton' under head wind ($\theta = 0°$) in the Reynolds number independent range is with $C_d = 0.12$ about 25% smaller than that of 'Aeolos'. Thrust, i.e. negative drag, is experienced by a 'Proton' rider if the apparent wind attacks at angles $\theta \geq 27°$ for $Re = 0.7 \cdot 10^5$, or at $\theta \geq 30°$ independent of the Reynolds number. The maximum thrust for the angles of wind attack investigated herein was found at $\theta = 52°$. For the 'Proton' the strength of the thrust appears to be sensitive to the angle of wind attack. A strong thrust is observed only in a relatively narrow band around the angle belonging to the maximum thrust.

GALA e.V., Karlsruhe, Germany, ISBN 978-3-9816764-8-8

Velocity Fields

Fig. 5. shows an instantaneous 2D velocity vector field in the vertical plane (x-z) at the spanwise-central axis of the velomobile 'Proton' for approach flow under θ = 0° angle of attack. Blue arrows indicate regular velocity vectors and green arrows substitute velocity vectors which were determined based on their neighboring velocity field since they did not comply with the validation criterion set in the PIV analysis. The presented snapshot is, based on a visual inspection of the velocity vector field time series, deemed representative for the flow around the velomobile. The velocity vectors indicate attached flow along the top faces of the velomobile (bonnet, windscreen, cabin roof). Flow separation and reverse flow is evident only at the rear side, below and leeward of the position indicated by '3' in the insert. The flow separation is attributed to the relatively sharp edge at this location, being a classical condition for flow separation.

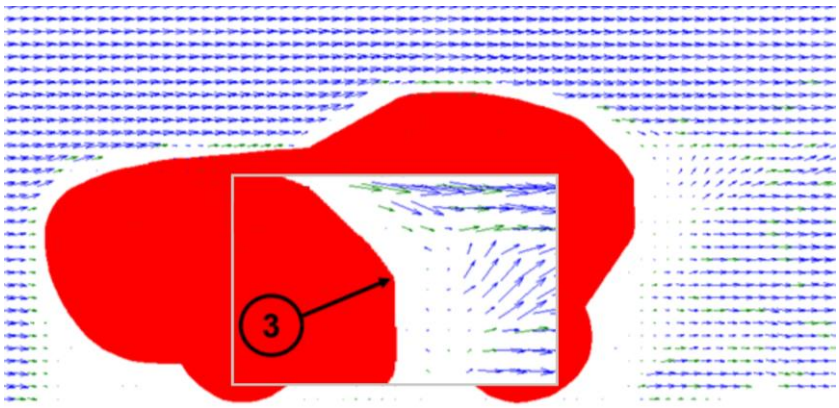

Fig. 5: Instantaneous 2D velocity vector field in vertical plane (x-z) at spanwise-central axis of the velomobile 'Proton' for approach flow under θ = 0° angle of attack at V_a = 20 m/s (Re = $0.94 \cdot 10^5$).

An instantaneous flow field in the horizontal plane (x-y) at the height of the maximum width of the velomobile is shown in Fig. 6. The velocity vectors evidence attached flow along the side face of the velomobile. In the rear zone, neither flow separation nor recirculation is suggested by the velocity vectors. However, their meaningfulness is limited since they are substitute vectors (green arrows).

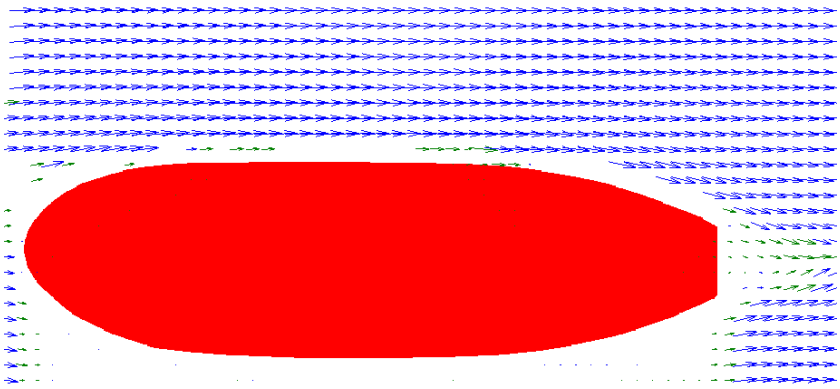

Fig. 6: Instantaneous 2D velocity vector field in horizontal plane (x-y) at height of maximum width of the velomobile 'Proton' for approach flow under θ = 0° angle of attack at V_a = 20 m/s (Re = $0.94 \cdot 10^5$).

The absence of flow separation at the top and side faces of the velomobile for an angle of wind attack of θ = 0° provides further evidence for the presence of a Reynolds number independent flow field at Re = $0.94 \cdot 10^5$. A drag reduction due to a delay of flow separation at increased Reynolds numbers is only possible if a separation, either at the top or side face, would occur in the present flow state, which is however not the case. Hence, the question whether or not a drag crisis occurs at higher Reynolds numbers as raised in the context of the presentation and analysis of drag force coefficients (Fig. 3 and 4), can, for wind attack under θ = 0°, be denied. Representative instantaneous velocity vector fields in the horizontal plane (x-y) for different angles of wind attack are provided in the left column of Fig. 7 in panels a, c, e. None of the instantaneous vector plots evidences flow separation at the side face of the velomobile. However, with increasing angle θ, the number of substitute velocity vectors (green arrows) increases in the region close to the surface, limiting the meaningfulness of the PIV analysis in the immediate vicinity of the velomobile.

GALA e.V., Karlsruhe, Germany, ISBN 978-3-9816764-8-8

On the right side of Fig. 7, in panels b, d, f, average images, based on 2,500 PIV raw images, are shown. For angles of wind attack of θ = 20° and θ = 30° dark elongated patched (stripes) appear next to the side face in the last third of the velomobile. The appearance of dark patches is attributed to the absence of tracer particles in rapidly rotating vortices which originate form flow separation at the side face of the velomobile. The rapidly rotating vortices appear dark because the tracer particles are ejected from their cores due to the centrifugal force. Based on this observation it is concluded that flow separation at the downstream-oriented side face of the 'Proton' emerges at an angle of wind attack 10°< θ < 20°.

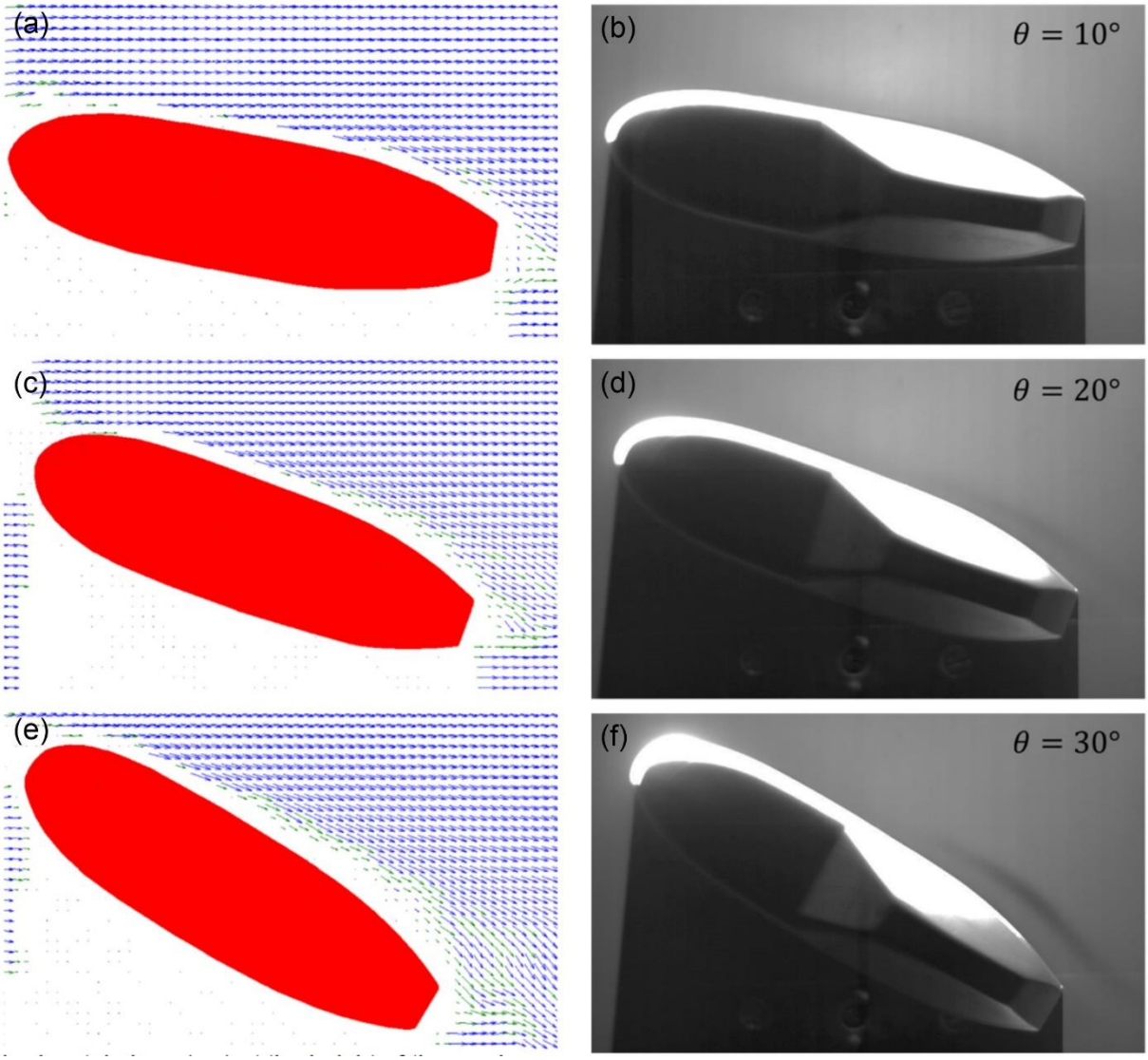

Fig. 7: Instantaneous 2D velocity vector field in horizontal plane (x-y) at height of maximum width of 'Proton' at Re = $0.94 \cdot 10^5$ (left); corresponding averaged raw images (right).

Summary and Conclusions

The wind tunnel studies performed at the scaled models of the velomobiles 'Aeolos' and 'Proton' revealed the following aerodynamic characteristics:

- Drag coefficients C_d of 'Aeolos' and 'Proton' asymptotically approaching, for most angles of wind attack, a constant value for Re > $0.9 \cdot 10^5$ and for Re > $1.2 \cdot 10^5$, respectively, providing evidence for Reynolds number independency at the scaled models.
- Decreasing drag coefficients with increasing angles of wind attack (at low to moderate angles θ ≤ 50°),

GALA e.V., Karlsruhe, Germany, ISBN 978-3-9816764-8-8

- Sail effect, i.e. thrust due to negative drag, for angles of wind attack $\theta \geq 30°$ for 'Aeolos' and $\theta \geq 27°$ for 'Proton' at all Reynolds numbers corresponding to realistic full-scale riding conditions,
- Maximum thrust at $\theta = 50°$ at $Re = 1.18 \cdot 10^5$ for 'Aeolos' and $\theta = 52°$ for 'Proton' with drag coefficient $C_d = -0.51$ and $C_d = -0.63$, respectively, being approximately 3 times and 5 times larger in magnitude than the corresponding drag coefficient for head wind ($\theta = 0°$),
- Flow separation at the side face of 'Proton' emerging at an angle of attack between 10° and 20°,
- Absence of flow separation at the top and side face of 'Proton' for $\theta = 0°$; flow separation and recirculation occurring only at the rear face.

Regarding the Reynolds number sensitivity, no general conclusive statements can be made for the velomobiles based on the available data. However, the absence of flow separation at the 'Proton' at wind-parallel faces for head wind ($\theta = 0°$) provides further evidence for the presence of a Reynolds number independent flow field at $Re = 0.94 \cdot 10^5$ and larger.

References

Dantec Dynamics, 2013: DynamicStudio User's Guide, Version 3.40, 660 pp

Fuchs, A., 1998: Trim of aerodynamically faired single-track vehicle in crosswinds. Proc. 3rd European Seminar on Velomobiles, p 134–156

Gromke, C., 2018: Wind tunnel model of the forest and its Reynolds number sensitivity. J. Wind Eng. Ind. Aerodyn. 175:53–64

Gromke, C., Ruck, B., 2018: On Wind Forces in the Forest Edge Region during Extreme Gust Passages and Their Implications for Damage Patterns. Bound.-Layer Meteorol. 168:269–288

Gross, A.C., Kyle, C.R., Malewicki, D.J., 1983: The Aerodynamics of Human-Powered Land Vehicles. Scientific American 249:142–152

IHPVA, 2019: IHPVA Official Speed Records. Index of Records. International Human Powered Vehicle Association, http://www.ihpva.org/hpvarech.htm

Kyle, C.R., Weaver, M.D., 2004: Aerodynamics of human-powered vehicles. Proceedings of the Institution of Mechanical Engineers, Part A: Journal of Power and Energy 218:141–154

Marzullo, O., 2022: Aerodynamic characteristics of single-track velomobiles under various crosswind conditions, MSc thesis, Karlsruhe Institute for Technology KIT, 123 pp

Rasmussen, C.G., Eick, J., 2005: Survival of the fittest. Proc. 5th European Velomobile Seminar 2005, Germersheim/Germany, p 99–104

Rasmussen, C.G., 2009: Velomobile aerodynamics – side wind effect and operation limits. Proc. 6th Seminar on Velomobile Design, 8 pp

Weaver, M., 1994: The Cutting Edge streamlined bicycle. Human Power: The Technical Journal of the International Human-Powered Vehicle Association 11:17–23

GALA e.V., Karlsruhe, Germany, ISBN 978-3-9816764-8-8